

RAL-94-012

Science and Engineering Research Council

Rutherford Appleton Laboratory

Chilton DIDCOT Oxon OX11 0QX

RAL-94-012

Results from the H1 Experiment at HERA

J Dainton

January 1994

COPY 2 R61 RB 23
ACCN: 221364

Science and Engineering Research Council

"The Science and Engineering Research Council does not accept any responsibility for loss or damage arising from the use of information contained in any of its reports or in any communication about its tests or investigations"

RAL 94 -
January 1994

Results from the H1 Experiment at HERA

John Dainton

*Department of Physics,
University of Liverpool,
P O Box 147, Liverpool L69 3BX, UK
and
DESY
22603 Hamburg, Notkestrasse 85, Germany*

for the H1 Collaboration at HERA

I. Phys. Inst. Aachen, III. Phys. Inst. Aachen, Univ. Birmingham, Inter-Univ. Inst. for High Energies Brussels, Rutherford Appleton Laboratory, Inst. for Nucl. Phys. Crakow, Univ. California Davis, Univ. Dortmund, DAPNIA Saclay, Univ. Glasgow, DESY-Hamburg, I. Inst. Univ. Hamburg, II. Inst. Univ. Hamburg, Phys. Inst. Univ. Heidelberg, Inst. für Hochenergiephysik Univ. Heidelberg, Univ. Kiel, Inst. Exp. Phys. Kosice, Univ. Lancaster, Univ. Liverpool, Queen Mary and Westfield College Univ. London, Univ. Lund, Univ. Manchester, ITEP Moscow, Lebedev Inst. Moscow, MPI München, LAL Orsay, Ecole Polytechnique, Univ. Paris VI and VII, Inst. Phys. Praha, Charles Univ. Praha, INFN and Univ. Roma, Univ. Wuppertal, DESY-Zeuthen, ETH Zürich, Univ. Zürich

Invited talk at the XVI International Symposium on Lepton-Photon Interactions, Cornell University, Ithaca, USA, August 1993

Results from the H1 Experiment at HERA

John Dainton

*Department of Physics,
University of Liverpool,
P O Box 147, Liverpool L69 3BX, UK
and
DESY
22603 Hamburg, Notkestrasse 85, Germany*

for the H1 Collaboration at HERA

I. Phys. Inst. Aachen, III. Phys. Inst. Aachen, Univ. Birmingham, Inter-Univ. Inst. for High Energies Brussels, Rutherford Appleton Laboratory, Inst. for Nucl. Phys. Crakow, Univ. California Davis, Univ. Dortmund, DAPNIA Saclay, Univ. Glasgow, DESY-Hamburg, I. Inst. Univ. Hamburg, II. Inst. Univ. Hamburg, Phys. Inst. Univ. Heidelberg, Inst. für Hochenergiephysik Univ. Heidelberg, Univ. Kiel, Inst. Exp. Phys. Kosice, Univ. Lancaster, Univ. Liverpool, Queen Mary and Westfield College Univ. London, Univ. Lund, Univ. Manchester, ITEP Moscow, Lebedev Inst. Moscow, MPI München, LAL Orsay, Ecole Polytechnique, Univ. Paris VI and VII, Inst. Phys. Praha, Charles Univ. Praha, INFN and Univ. Roma, Univ. Wuppertal, DESY-Zeuthen, ETH Zürich, Univ. Zürich

ABSTRACT

First results from the H1 experiment at the high energy electron-proton (ep) collider HERA are presented. Based on an integrated ep luminosity of about 25 nb^{-1} accumulated during the first data taking period in 1992, first measurements of soft and hard photoproduction and of deep inelastic ep scattering (DIS) have been made. The total photoproduction cross section is measured to be $156 \pm 2 \pm 18 \text{ (sys)} \mu\text{b}$ at $\langle W_{\gamma p} \rangle = 197 \text{ GeV}$. Hard partonic dynamics in photoproduction are observed, and resolved photon contributions inferred in which first hints of interactions involving gluonic components of real photon structure are seen. A measurement of the proton structure function $F_2(x, Q^2)$ in the new kinematic region of Bjorken x (x_{Bj}) between $\sim 10^{-4}$ and $\sim 10^{-2}$ is presented showing a substantial rise as x_{Bj} decreases. Measurements of the characteristics of hadronic energy flow in such low x DIS events are presented, and a class of events with a large pseudorapidity interval devoid of hadronic energy close to the proton beam direction is reported.

INTRODUCTION

The H1 experiment at the HERA high energy electron-proton (ep) collider is a collaboration of about 340 physicists from 36 institutes. The collaboration was formed in 1985, submitted a Letter of Intent to the DESY Physics Research Committee (PRC) in 1985 [1], and then a Technical Proposal in 1986 [2]. Following approval by the PRC and construction in the collaborating laboratories, the experiment was installed and was operational in the North Hall at HERA by Spring 1991, since when it has taken first cosmic ray data, and (from June 1992) ep collision data. The results presented here are in the main based on analysis of an integrated luminosity of about 25 nb^{-1} accumulated during the first data taking period in summer and autumn 1992 in which 26.7 GeV energy electrons collided head-on with 820 GeV protons (CMS energy $\sqrt{s} = 296 \text{ GeV}$).

The following includes a brief description of the H1 experiment, the main emphasis being on aspects related to the unique ep collider configuration at HERA, followed by presentation and discussion of new results concerned with photoproduction (γp) and deep inelastic (ep) physics.

THE H1 EXPERIMENT

The H1 experiment (FIG. 1) follows the philosophy of most collider experiments to date, namely as hermetic as possible measurement of hadronic energy flow, charged track reconstruction, and lepton (electron and muon) identification [3]. The notable distinction of experiments at HERA is the enhanced instrumentation in the "forward" proton direction due to the asymmetry of the electron and proton beam energies, respectively 26.7 GeV and 820 GeV . The reasons for this asymmetry are attributable both to machine physics limitations and to detection efficiency. Electron energy is limited in the usual way because of synchrotron radiation losses in the electron ring, but also because adequate acceptance, i.e. measurable scattering angle, for scattered electrons of intermediate Q^2 (~ 5 to 100 GeV^2) is desirable. The implications for the detector configuration are obvious, namely enhanced segmentation and coverage in the forward (proton beam) direction, and the best possible electron detection extending down to the backward (electron beam) direction, that is down to the smallest electron scattering angles.

The H1 detector components are summarised in Table 1 in which are also listed salient parameters specifying performance in 1993 running. All components listed are presently operational during data taking.

The backbone of H1 is the liquid argon calorimeter (LAr) which comprises electromagnetic (EM) and hadronic (HAC) sectors [4]. Its notable features include dense lateral and longitudinal segmentation. This is not only for good angular precision, but also is to facilitate the best possible energy resolution ($\sim 51\%/\sqrt{E(\text{GeV})}$) by means of energy weighting using the spatial distribution of energy deposition to equalise overall hadronic and electromagnetic response. Also vital to precision physics is stability and precision of the absolute energy scale of these responses, the former of which has varied by $\leq 0.5\% \text{ year}^{-1}$ since installation in 1991, and the latter of which is presently established to $\pm 3\%$ (EMC) and $\pm 7\%$ (HAC) in operation and is limited presently only by available statistics.

The backward electromagnetic calorimeter (BEMC) is optimised for detection and measurement of electrons (and positrons) scattered through intermediate angles ($\sim 4 \leq Q^2 \leq \sim 100\text{ GeV}^2$). It is a "conventional" scintillator and lead absorber device read out with wavelength shifter. Careful calibration, following test beam measurements, presently yields an energy resolution of $\sim 10\%/\sqrt{E(\text{GeV})}$, a precision of the energy scale of $\pm 2\%$, and an impact position resolution of $\sim 1.4\text{ cm}$ before clusters are associated with charged hits in the proportional chamber planes (BPC) which precede it. Very nearly all scattered electrons in the neutral current (NC) DIS events discussed here are detected in the BEMC.

The charged track detectors in H1 consist of the Central Track Detectors (CTD) and the Forward Track Detectors (FTD). Each consists of a hybrid of drift and proportional chambers (MWPCs). The CTD drift chambers measure r and ϕ in two high precision "jet chamber" like devices (CJC1 and CJC2) sandwiching, and sandwiched by, z drift chambers (CIZ, COZ). The FTD drift chambers measure $r\phi$ and r . Together CTD and FTD provide precision track reconstruction over a substantial range of polar angle ($\sim 6^\circ \leq \theta \leq \sim 155^\circ$) with fast inter-bunch signals for triggering and timing. Both these track detectors and the liquid argon calorimeter are inside a large radius solenoid. The CTD and FTD thus sit in a uniform axial magnetic field with negligible transverse field components.

Measurement of the charge deposited on the sense wires in both the CTD and FTD drift chambers enables particle identification by means of track ionisation dE/dx . In the FTD, where the track density is especially large, e/π discrimination is further enhanced by means of the detection of transition radiation (TR) in the drift chambers. When the latter is combined with the traditional method of comparing parameters of track and LAr EMC energy deposition, excellent e/π discrimination ($\leq 10^{-3}$ hadron contamination) is possible over the polar angle range $\sim 6^\circ \leq \theta \leq \sim 171^\circ$.

The iron flux return yoke is instrumented with Luranyl streamer tubes for muon detection and measurement in a nowadays standard way ($C\mu$). Additional analogue read-out facilitates detection of hadronic energy escaping from rear of the HAC. For the same reasons as electron identification is enhanced in the forward tracking region, muon discrimination is improved using a forward muon spectrometer composed of drift chambers and toroidal

magnetic field ($F\mu$). The result is excellent muon detection ($\leq 10^{-3}$ hadron rejection) over the polar angle range $\sim 4^\circ \leq \theta \leq \sim 171^\circ$.

TABLE 1. Essential Components of the H1 Experiment

LAr Calorimeter		EMC(Pb)	HAC(steel)
• central+forward $4 < \theta < 155^\circ$	• trans seg ^a 4×4 cm	8×8 cm	
• stability $\leq 0.02\%$ yr ⁻¹	• contain ^t $20 - 30X_0$	$4.8 < \lambda_{abs} < 8$	
• noise $10-30$ MeV ch ⁻¹	• channels $30,784$	$13,568$	
• trigger tower ≥ 1.2 GeV	• σ_E/E $12\%/\sqrt{E} \oplus 1\%$	$50\%/\sqrt{E} \oplus 2\%$	
• $E_{Tmiss} \geq 3$ GeV			
Backward EM Calorimeter			
BEMC (Pb+scintillator) + BPC (MWPC)			
• transverse seg ^a 16×16 cm	• 4 wire planes		
• $\sigma_E/E = 10\%/\sqrt{E} \oplus 3\%$	• $\sigma_{xy} = 2.5/\sqrt{12}$ mm		
• backward $150 < \theta < 174^\circ$	• backward $155.5 < \theta < 174.5^\circ$		
Charged Track Detectors			
Superconducting Solenoid $B=1.14$ T $\Delta B/B < 2\%$			
Central (CTD)		Forward (FTD)	
• $25 < \theta < 155^\circ$	• "jet" drift chamber $21 < r < 85$ cm	• $6 < \theta < 25^\circ$	• drift radial+planar $1.3 < z < 2.4$ m
• 2640 sense wires	• $\sigma_{r\phi} = 170$ μ m $\sigma_{dE/dx} \sim 10\%$	• 1728+1152 sense	• $\sigma_{r\phi} = 170$ μ m $\sigma_{xy} = 210$ μ m
• z chambers $\sigma_z = 2$ mm	• trigger MWPCs $\Delta t < 96$ ns	• TRD: TRs+radial drift ch ^a	• trigger MWPCs $\Delta t < 96$ ns
• $\sigma_{1/p} \leq 0.8\%$ GeV ⁻¹		• $\sigma_{1/p} \geq 3\%$ GeV ⁻¹ $\Delta z \leq 1$ m	
Instrumented Iron			
• central streamer + forward drift + toroidal B $4 < \theta < 171^\circ$			
Time of Flight			
• scintillator $\sigma_t \sim 1$ ns			

The HERA interaction environment is complicated not only by substantial electron beam synchrotron radiation and proton beam halo and secondaries, but also by the severe timing requirements of a bunch crossing interval of only 96 ns. Apart from the use of MWPC signals, an essential tool for out of time background rejection is the large area time of flight (ToF) system of scintillators, located behind the BEMC, which discriminate against proton background originating upstream (proton beam) of the interaction region.

Last, but by no means least, are luminosity measurement and small angle electron detection in the "luminosity monitor" (Lumi). Two arrays of radiation hard crystal detectors (total absorption of Cerencov light) are positioned 33 m and 103 m downstream (electron beam) for electron and photon detection respectively, and for energy measurement. Luminosity is determined from the Compton process

$$ep \rightarrow ep\gamma$$

in which the rate for $e\gamma$ coincidences is compared with the (low Q^2) QED expectation. Electrons "tagged" in the electron detector in coincidence with activity in H1 are candidate triggers for very low Q^2 electroproduction ($Q^2 \leq \sim 0.013$ GeV²), and form the basis of most of the photoproduction physics discussed below.

Throughout 1992 data taking HERA operated with only ~ 10 electron and proton bunches and a typical peak luminosity of $\sim 3 \times 10^{28}$ cm⁻² s⁻¹. In about 3 months data taking ~ 25 nb⁻¹ integrated luminosity were

accumulated. HERA now operates with 84 colliding electron and proton bunches, another 10 electron “pilot” bunches in which the corresponding proton r.f. bucket is empty, and a further 6 proton “pilot” bunches. The pilot bunches are important for an understanding of beam-gas, beam-wall and beam-halo backgrounds. This year the peak luminosity has reached nearly 10% of design, namely $\sim 10^{30} \text{ cm}^{-2} \text{ s}^{-1}$, and in a typical weekend it is possible to accumulate integrated luminosity equivalent to 3 months running in 1992. The analysis of these 1993 data is still of course underway.

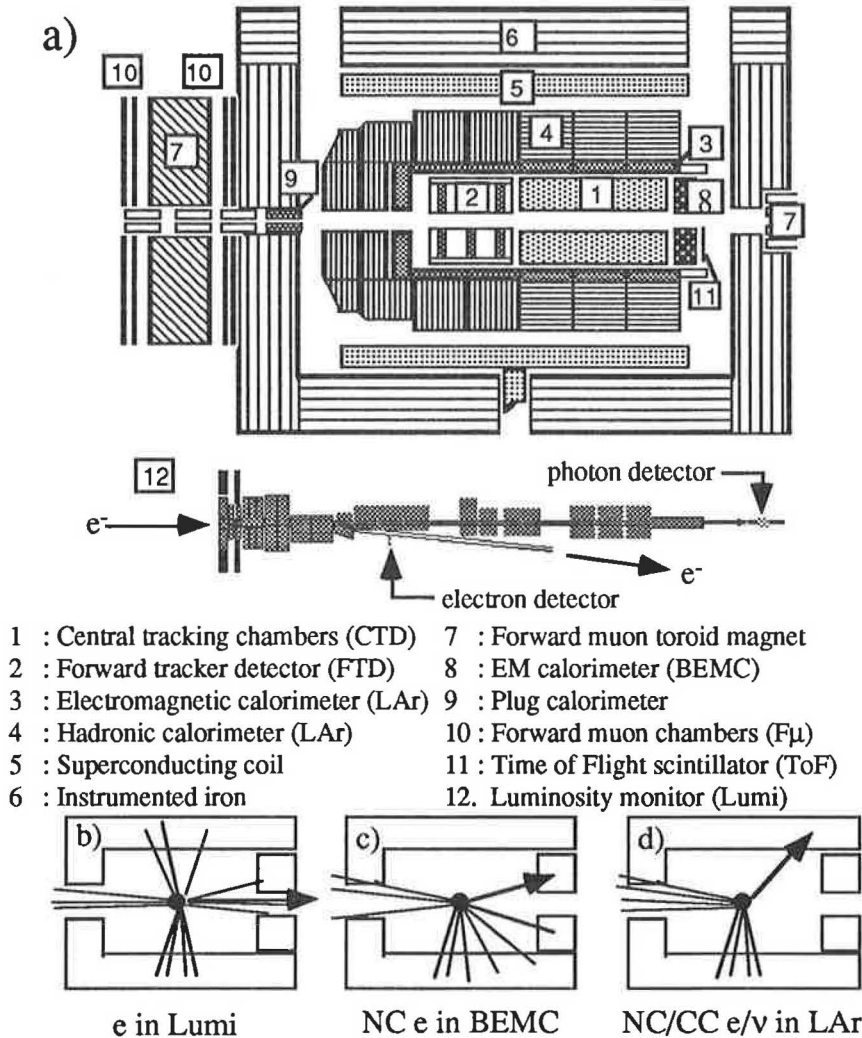


FIG. 1. a) Schematic r - z view of the H1 experiment at HERA in which the asymmetry due to the different incident electron ($\sim 30 \text{ GeV}$ from the left) and proton ($\sim 820 \text{ GeV}$ from the right) energies, is manifest. Note that the luminosity monitor, downstream in the electron direction, is not to scale. b) c) d) Schematic ep interactions in H1: b) photoproduction with scattered electron in the beam pipe possibly detected in Lumi, c) NC DIS with scattered electron detected in BEMC, d) NC or CC DIS with final state electron detected in LAr or with substantial imbalance in E_T ; proton remnant fragments may or may not be detected close to the forward beam pipe.

A vital aspect of physics at HERA is triggering. Table 2 summarises the H1 set-up. ToF, CTD and FTD MWPCs, CTD CJC, LAr, Cμ and Fμ, and Lumi all contribute to trigger decisions at level 1, that is provide signals that identify unambiguously the bunch crossing in which the event occurred ($< 96 \text{ ns}$). In essence ToF “out of time” veto, MWPC rays for z (beam axis) vertex estimate, and Lumi energy are used to reject

background. Lumi energy, LAr transverse energy E_T and missing E_T (ΔE_T), $C\mu$ and $F\mu$, CJC $r\phi$ and MWPC z vertex are combined to form physics motivated triggers. There follow in principle trigger levels 2, 3 and 4. When implemented, levels 2 and 3 will run in “real” time on “pipelined” data using programmable hardware. Level 4 is a farm of parallel RISC processors on which are run the full reconstruction codes, the results of which form the basis of further background rejection.

TABLE 2. Schematic of H1 Trigger and on-line event Filter

0	2 μ s	20 μ s	800 μ s	100 ms	
now	L1	L2	L3	L4	
dead time	< 96ns	20 μ s	<800 μ s		
rate now	60			5 - 10	Hz
rate future	1000	100	5	Hz
how	sub-det ^r hardware	front-end hardware	front-end software	event filter 15 RISC 300 Mips	
purpose	pipeline stop	read-out start	event build start	data log & reject	
means	ToF veto MWPCs z vertex e-tag E_e		} background rejection } physics calo $E_T + \Delta E_T$ $C\mu + F\mu$ drift chamber $r\phi$ MWPCs z vertex		

An overall impression of why H1 is the way it is, is given by considering the topological characteristics of the essential physics. Photoproduction interactions, that is very low Q^2 electroproduction for which the incident electrons are scattered through extremely small angle and are sometimes detected in the Lumi detector, are observed in H1 to the extent that they have adequate transverse momentum p_T (with respect to the beam pipe) in the final state to trigger and subsequently reconstruct (FIG. 1b). Neutral current (NC) deep inelastic (DIS) ep physics is manifest at intermediate or large Q^2 with a reconstructed electron in the BEMC or LAr respectively and final state hadronic energy flow balancing kinematically in p_T (FIG. 1c). Charged current (CC) DIS ep physics is manifest at large Q^2 as hadronic energy flow with a large p_T imbalance (FIG. 1d). A substantial fraction of the ep collision energy is lost in the beam pipe in the form of a proton remnant in both NC and CC DIS. Most of the quantitative results quoted here are concerned with the first, relatively low, luminosity data at HERA, and thus with NC processes.

ELECTRON-PROTON PHYSICS AT HERA

It is appropriate here to state briefly the framework in which ep physics at the HERA ep collider is carried out. FIG. 2 and the following equations summarise how the essential kinematic variables \sqrt{s} , y , Q^2 and x_{Bj} are determined from the measured electron scattering angle $\pi-\theta$ (note the convention $\theta = 0$ in the proton beam direction), the initial and final electron energies E_e and E_e' respectively, and the proton beam energy E_p :

$$s = 4E_e E_p \quad (1)$$

$$y = 1 - E_{e'}/E_e \sin^2 \theta/2 \quad (2)$$

$$Q^2 = 4E_e E_{e'} \cos^2 \theta/2 \quad (3)$$

$$x_{Bj} = Q^2/y_s = Q^2/(Q^2+W^2) \quad (4)$$

Given the overall ep energy scale \sqrt{s} , y and Q^2 specify the scattered lepton (electron or neutrino) energy and angle, and thus, in the Standard Model, also the space-like characteristics of the exchanged electroweak quantum (NC γ and Z^0 , CC W^\pm). The invariant mass of the total hadronic final state is W . A variable x is often taken to be the momentum of the piece (partonic or otherwise) of the incident proton as a fraction of the latter's momentum (neglecting transverse momentum) which interacts with the incident electron. When the piece of the proton interacts elastically with the incident electron, Bjorken- x x_{Bj} in (4) above is x . This is the case in the parton model (QPM, i.e. zeroth order QCD). In QCD x_{Bj} is the momentum fraction of the quark coupling to the space-like electroweak quantum.

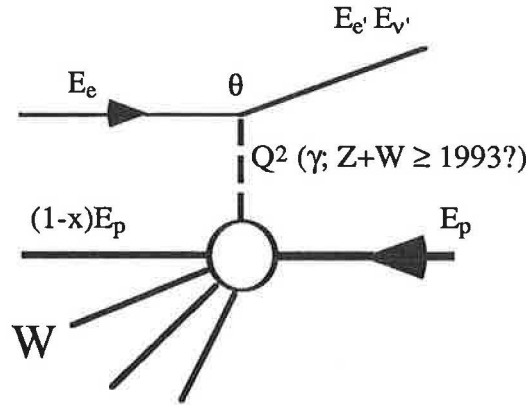


FIG. 2. Kinematics of electron-proton (ep) physics at HERA in the Standard Model: an electron of energy E_e interacts inelastically with a proton of energy E_p by means of the exchange (in the Standard Model) of a gauge boson (γ , Z^0 , W^\pm); the lepton (electron or neutrino) scatters through an angle $180^\circ - \theta$, the hadronic invariant mass is W ; the CMS ep collision energy is \sqrt{s} .

Photoproduction processes are studied by measuring NC interactions for which $\theta \rightarrow 180^\circ$, $Q^2 \rightarrow 0 \text{ GeV}^2$, and the scattered electron is in the beam pipe and sometimes measured in the Lumi detector. Then $y (= 1 - E_{e'}/E_e)$ is the incident photon energy as a fraction of the incident electron energy. DIS processes require $180^\circ - \theta$ large enough either for the scattered lepton to be measured with $Q^2 \geq \sim 4 \text{ GeV}^2$ in either the BEMC or LAr calorimeters (NC), or for there to be adequate rate i.e. $Q^2 \geq \sim M_W^2$ (CC). Now

$$\cos \theta^* = 2y - 1 \quad (5)$$

where θ^* is the CMS scattering angle of the lepton in its partonic sub-process.

PHOTOPRODUCTION

Phenomenology

The phenomenology of hadronic photoproduction is well established, following nearly 30 years' development. The total hadronic interaction cross section, whose value is itself of great theoretical and

experimental significance, is conveniently split into three classes based on experimental criteria: i) soft, vector dominance model (VDM) dominated, hadronic physics (FIG. 3a), ii) hard hadronic physics in which the photon interacts much like a conventional hadron with the proton, that is via perturbative QCD dynamics between partonic constituents (FIG. 3c), and iii) hard electroweak physics in which the photon couples like a Standard Model gauge boson to (electrically charged) proton constituents (FIG. 3b).

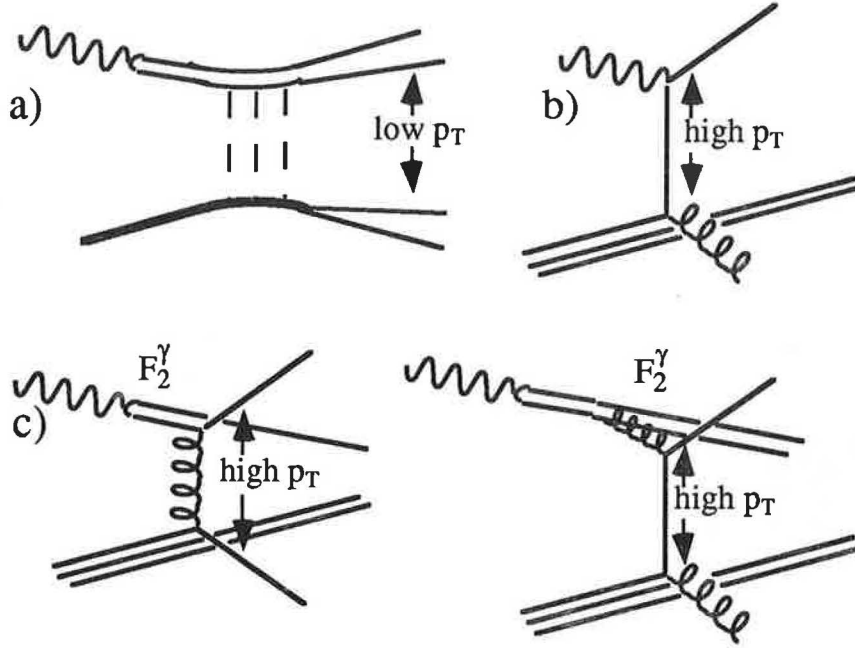


FIG. 3. Photoproduction phenomenology: a) soft (peripheral) γp interactions - the incident photon interacts hadronically after “hadronising” at low p_T relative to its momentum into vector mesons (VDM model) with low 4-momentum transfer excitation of either or both of the incident photon and proton; one or two limited p_T soft jets of hadrons are thus produced; b) $O(\alpha_s)$ QCD dynamics due to the “direct” interaction of the incident photon with an electrically charged parton (quark) in the proton giving rise to at least two high p_T jets plus only one low p_T “beam pipe” remnant from the proton; c) leading order QCD dynamics of hard γp photoproduction due to the interaction of a “resolved photon”; partons from the hadronised photon and from the proton interact at high p_T producing at least two high p_T parton jets plus two low p_T remnants; the structure of the hadronised photon is partly calculable perturbatively and is partly phenomenological (VDM).

Soft VDM physics is well established from many lower energy measurements (average CM energy up to $\langle W_{\gamma p} \rangle \sim 20 \text{ GeV}$) and their comparison with soft hadronic physics. At HERA energies ($\langle W_{\gamma p} \rangle = 197 \text{ GeV}$) it mainly gives rise to low p_T (peripheral) jets associated with inelastic collisions in which either or both of the incident photon and proton are excited hadronically and inelastically to higher mass resonant states. The contributions to the total γp cross section of such processes are large at lower energies.

Hard photoproduction has been observed as “a tail” in hadronic p_T and E_T spectra (with respect to the γp axis) in lower energy measurements [5]. Until now it has not been possible to distinguish unambiguously hard photoproduction processes of type ii) and type iii) above because of the lack of available final state phase space. The distinction between them is motivated more by a decade of theoretical work on QCD photon structure [6] and by measurement of the hadronic photon structure function F_2^γ in deep inelastic $e\gamma$ scattering at e^+e^- experiments [7]. There it has clearly been established that the photon has hadronic structure much as expected in QCD due to “vacuum polarisation like” contributions involving quarks and gluons. At low p_T relative to the photon, these contributions are non-perturbative, are therefore presently incalculable, and are phenomenologically well parametrised by VDM. But an additional contribution, sometimes referred to as the “anomalous QCD

component" of photon structure, is calculable perturbatively, and its main features are observed at high p_T and at high Q^2 in deep inelastic $e\gamma$ interactions [7]. Hard γp interactions at high p_T of type ii) therefore involve an interaction in which the photon structure is probed by the (now hadronic) high p_T of the collision, much like a normal hadron. Therefore only part of the incident photon momentum is involved in the high p_T interaction, and, exactly as for the proton in the interaction, there remains an hadronic remnant at low p_T (along the electron beam direction). Such processes are termed "resolved" photon collisions.

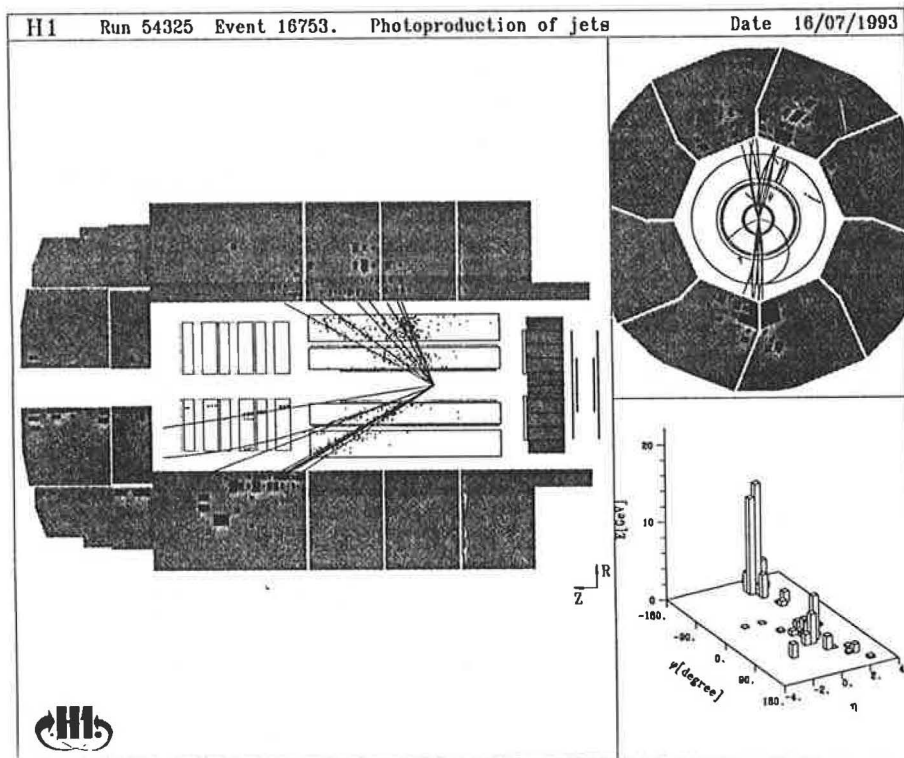


FIG. 4. A "typical" high p_T photoproduction event showing a clear 2-jet topology, kinematically balanced, and with no evidence for any photon fragment at low p_T in the electron beam direction.

Interactions between the incident photon and charged partons (quarks) in the proton, so called "direct" photon interactions, are of type iii). Clearly they are characterised by no low p_T remnant from the photon. Their dynamics do not depend in any way on the photon structure function. Experimentally direct real photon interactions with absence of a photon remnant have not yet been unambiguously observed, though "typical" high p_T events, such as in FIG. 4 in which 2-jet activity is clear and no photon remnant is apparent, are suggestive. Measurements at lower energy of inclusive hadron photoproduction, and quantitative comparison with purely hadronic interactions at the same energy, have shown that an excess of signal at high p_T in the former compared with the latter can be explained by the inclusion of a direct photon like contribution [5].

All quantitative understanding of high p_T photoproduction obviously also depends on proton structure, and is only meaningful if the parton content of the proton is known. For the kinematic region of present high p_T photoproduction measurements at HERA, systematic error due to uncertainty (especially at low Bjorken x) in the latter is found to be small.

Measurement of the Total Photoproduction Cross Section

Following the first measurement by H1 of the total hadronic photoproduction cross section using only 1.5 nb^{-1} integrated luminosity in 1992 [9], FIG. 5 shows the result using 21.9 nb^{-1} , namely $156 \pm 2 \pm 18 \text{ (sys)} \mu\text{b}$

($\langle W_{\gamma p} \rangle = 197 \text{ GeV}$)[†]. Also shown is the 1992 published result from the Zeus experiment [10]. There is no evidence for any unexpected dependence when lower energy measurements are extrapolated to this energy. Two parametrisations motivated by the dominance of soft (Regge framework) physics at low energy extrapolate well through the new measurements [11,12]. Further reduction of the (systematic dominated) errors on this measurement will go hand in hand with a better understanding of the mix of diffractive and non-diffractive contributions to hadronic photoproduction. Already, familiar components of hadronic production, such as “elastic” ρ photoproduction, are clearly seen in the data.

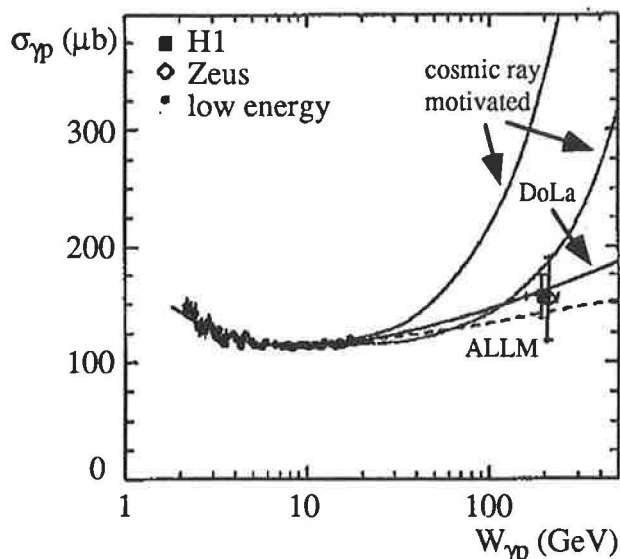


FIG. 5. Measurement of the total hadronic photoproduction cross section at γp CM energy 197 GeV ; also shown are low energy points, the published result from Zeus [10], and the extrapolations from low energy of Regge motivated models (DoLa [11] ALLM [12]) and models motivated by anomalies in cosmic ray air showers and built on the hypothesis of mini-jet production [37].

High p_T Photoproduction and Photon Structure

In 1992 with only the first 2 nb^{-1} of H1 data, it was possible to establish for the first time that the inclusive ep jet rate as a function of transverse energy E_T could not be explained by direct photon interactions alone but required the inclusion also of resolved photon interactions, and, soon after that, events with hadronic fragments at low p_T in the backward direction were also observed [8].

Further quantitative measurements of high p_T photon interactions are now well underway. FIG. 6 shows the unmistakable and classic evidence for hard scattering in photoproduction now at HERA γp energies, namely a tail in the p_T spectrum of charged tracks. Superimposed is a theoretical next to leading order (NLO) QCD expectation assuming that resolved photon processes dominate [14]. The normalisation of the latter is not yet matched properly to the pseudorapidity range of the measured cross section, but the shape of the spectrum is well reproduced. Perhaps more appealing is the comparison with the same spectrum (arbitrarily normalised) for charged hadrons from pp interactions at roughly the same CM energy [15]. It is clear that the high p_T tail is significantly more pronounced in γp induced processes than in hadron induced processes, as also observed in lower energy measurements [5].

[†] This measurement does not yet include a term in the Weizsaecker-Williams equivalent photon flux $O(m_e^2/Q^2)$ which is significant for electron scattering measurements at very small scattering angle and which amounts to an increase in photon flux of about 7% for forward electron detection in the H1 Lumi detector.

Of course the qualitatively convincing demonstration of parton dynamics in hard scattering is the observation of high p_T jet production. Two jet production is obvious in FIG. 4, underlining the point that only now at the γp CM energies possible at HERA are jet phenomena unambiguous in high p_T photoproduction physics, and therefore that the evidence for parton dynamics is now finally as indisputable in high energy photoproduction as it is in high energy hadroproduction. FIG. 7 shows the evidence for “two-jettiness” as a function of p_T scale, conveniently measured as calorimeter E_T . As the threshold in the latter is raised, the spectrum of the distance in azimuth $\Delta\phi$ of charged tracks from the leading particle in p_T shows an evolution towards a back-to-back peaking at $\Delta\phi = 0^\circ$ and 180° , classic “two-jettiness”.

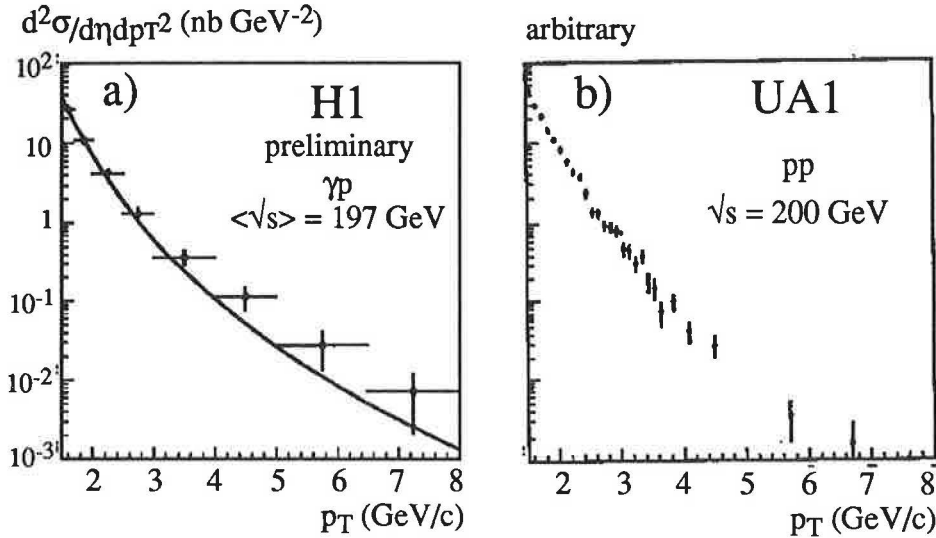


FIG. 6. a) Inclusive charged track p_T ep cross section (for tracks with $p_T > 1.5 \text{ GeV}$ and pseudorapidity $|\eta| < 1$) together with an arbitrarily normalised spectrum from a NLO QCD calculation of resolved photon interactions [14]; b) the same spectrum measured at the same CM energy with arbitrary normalisation and the same abscissa scale ($W = \sqrt{s} \sim 200 \text{ GeV}$) in pp interactions [15].

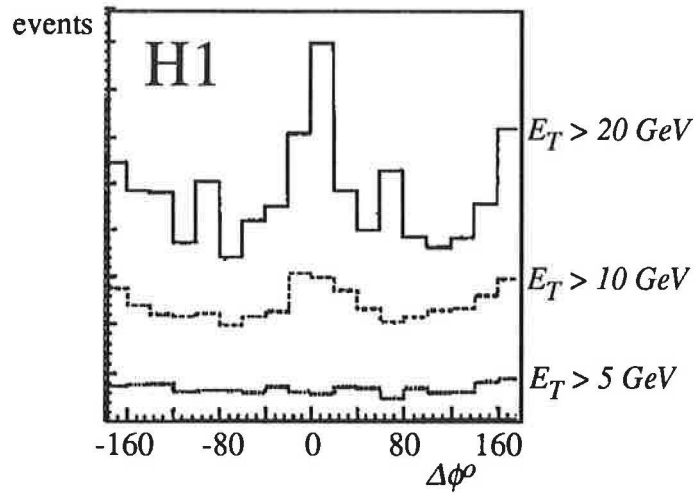


FIG. 7. Distribution of distance $\Delta\phi$ in azimuth ϕ of charged tracks in an event from the leading p_T charged track as a function of calorimeter E_T threshold, showing the development of back-to-back clustering characteristic of the kinematic balance of two-jet production with increasing E_T .

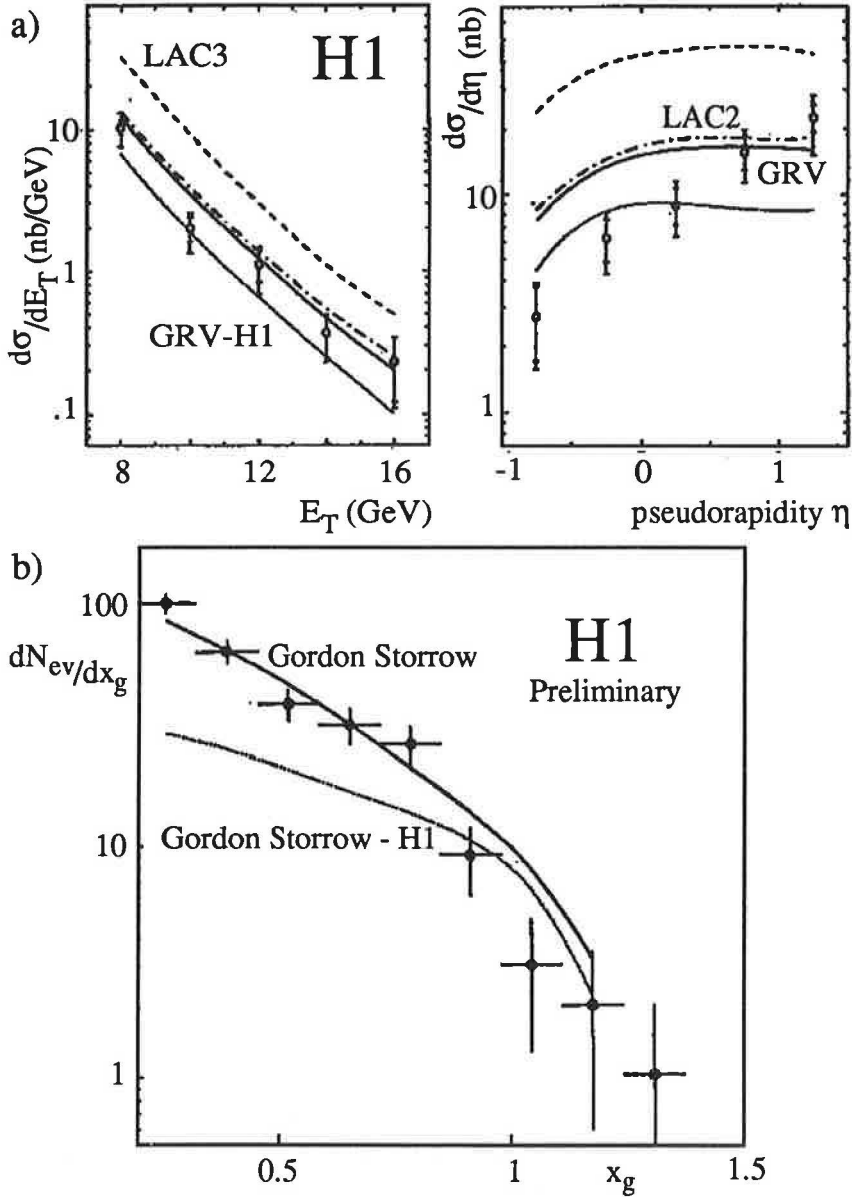


FIG. 8. a) Inclusive jet production cross section for photoproduction at CM energy $\langle W_{\gamma p} \rangle = 197 \text{ GeV}$ as a function of calorimeter E_T and pseudorapidity η with the expectations based on a LO QCD calculation with different choices (LAC2, LAC3, GRV, GRV-H1) of parton distribution functions (pdfs) for the photon (F_2^γ) [17]; note that an overall 40% systematic uncertainty remains in the scale of the cross sections; b) the inclusive event rate in H1 (uncorrected for acceptance) for hard photoproduction ($E_T > 5 \text{ GeV}$, $|\eta| < 2.5$) as a function of photon Bjorken-x x_g , together with the expectations based on a LO QCD calculation with different choices of pdfs for the photon (F_2^γ) [17]; in a) (b) GRV-H1 (Gordon and Storrow-H1) uses the GRV (Gordon and Storrow) QCD analysis for the pdfs but with the gluonic interaction cross section set to zero thereby demonstrating the sensitivity to the gluon content of the photon.

The cross section for inclusive jet production in ep interactions has been measured as a function of calorimeter E_T and pseudorapidity η in the laboratory using data in which the scattered electron is “tagged” in the Lumi detector. Jets are identified using a cone algorithm following the “Snowmass accord” (jet “radius” $R =$

$\sqrt{(\Delta\eta^2 + \Delta\phi^2)} \leq 1$) [16]. FIG. 8a shows the usual decrease of the cross section with E_T increasing to ~ 16 GeV, limited by present statistics, and that the η spectrum rises towards the forward (proton beam) direction [13]. When compared with what amounts to a LO QCD expectation for the hard parton sub-process, there is already sensitivity to different parton distribution functions (pdfs) in the (resolved) photon structure functions [17], and the intriguing possibility that the η dependence may be different from any present expectation. In particular, photon structure with substantial gluonic content (LAC3 [17]) at high x_γ (the Bjorken- x variable relevant to photon structure) already looks unlikely. More data and a better understanding of systematics will permit definitive discrimination between these phenomenological descriptions of photon structure, all of which are based on the QCD evolution of deep inelastic $e\gamma$ measurements at e^+e^- experiments.

The data have also been analysed for an x_γ dependence with the ultimate aim of unfolding a photon structure function from the hard scattering process. The "tagged" photoproduction sample is used in which the photon energy is thus known. Though the latter reduces statistics, it does eliminate background in the rather limited (on a HERA energy scale!) p_T reach of present integrated luminosity. Parton x_γ in the photon is measured using

$$x_\gamma = (E_{T1} e^{-\eta_1} + E_{T2} e^{-\eta_2}) / 2yEe' \quad (6)$$

where E_{Ti} and η_i are the transverse energies and pseudorapidities of each jet $i=1,2$. FIG. 8b shows the measured event rate as a function of x_γ together with the expectation of some of the different choices for pdfs extracted from QCD analyses of F_2^γ [17]. Much of our uncertainty of the latter is based on the fact that DIS $e\gamma$ measurements in e^+e^- experiments are sensitive to gluon content only indirectly through QCD evolution of F_2^γ , in contrast with high p_T photoproduction and real photon $\gamma\gamma$ processes. Once again, the choice of a large gluon content in F_2^γ at large x_γ is ruled out (LAC3). One of the pdf choices for F_2^γ which is compared with the data in FIG. 8b (Gordon and Storrow-H1) takes the description of F_2^γ and ignores any hard scattering of the (QCD evolved) gluon component. It is immediately clear that present measurements require the gluon hard scattering contribution at substantial x_γ and therefore by implication the gluon contribution to real photon structure, a result which is also emerging from new measurements at lower energy in high p_T real photon $\gamma\gamma$ physics in e^+e^- experiments at KEK [7]. This is confirmed in the jet cross sections in FIG. 8a) using different pdfs for F_2^γ (GRV-H1).

DEEP INELASTIC ELECTRON-PROTON SCATTERING

Kinematic Region and Phenomenology of First DIS Measurements at HERA

DIS lepton proton physics, and in particular the Q^2 and x_{Bj} dependences of the proton structure functions, are a cornerstone of modern particle physics. HERA takes DIS into completely new kinematic regions. The high ep CM energy \sqrt{s} (~ 296 GeV) and colliding beam design luminosity make possible deep inelastic measurements with two orders of magnitude increase in Q^2 . FIG. 9 summarises the kinematics in the $x_{Bj} - Q^2$ plane in terms of the scattered lepton and current direction. In general, hadronic energy flow will occur for rapidity between that of the current (struck) parton vector and the forward proton remnant (unmarked and towards the left in FIG. 9) in the proton beam direction (note the change of energy scale between final state lepton and current). To reach high Q^2 requires high integrated luminosity, which is yet to come from HERA. The present NC DIS data sample in H1 is shown superimposed, where it is clear that present measurements are accordingly somewhat limited in their Q^2 reach, but that the extremely large CM energy \sqrt{s} means that the ep data extend down to a new and fascinating kinematic region of proton structure, namely $10^{-4} \leq x_{Bj} \leq 10^{-2}$.

The importance of this new, uncharted, low x_{Bj} region of DIS is summarised in FIG. 10a, in which is shown a (debatable!) theoretical view in the $1/x_{Bj}$ and Q^2 plane of the kinematic domains appropriate and amenable to calculation [18]. Overlaid is again the H1 DIS sample which is seen to extend well beyond the theoretically familiar region of standard DGLAP [19] QCD evolution into regions where the gluon density is likely to dominate other parton contributions [20,21,22 and references therein].

Access to this new low x_{Bj} deep inelastic region for the first time forces careful consideration theoretically of the influence of the infra-red divergences which occur in QCD splitting at low x so that intuitively one

expects the proton structure function F_2 to rise somewhat with decreasing x_{Bj} . In practice these divergences give rise to large $\ln 1/x$ terms which have to be summed in understanding the (low) x_{Bj} dependence of F_2 . The sort of diagrams which one anticipates contributing to F_2 include the gluon dominated “ladder” with the possibility of splitting into isolated, color singlet, “limbs” by virtue of the non-abelian gluon self coupling, a “fan” diagram (FIG. 10b). One may go further and surmise that the resulting high gluon density in the proton will give rise to recombination effects and to parton screening, both of which will ultimately inhibit any rise of F_2 with decreasing x_{Bj} .

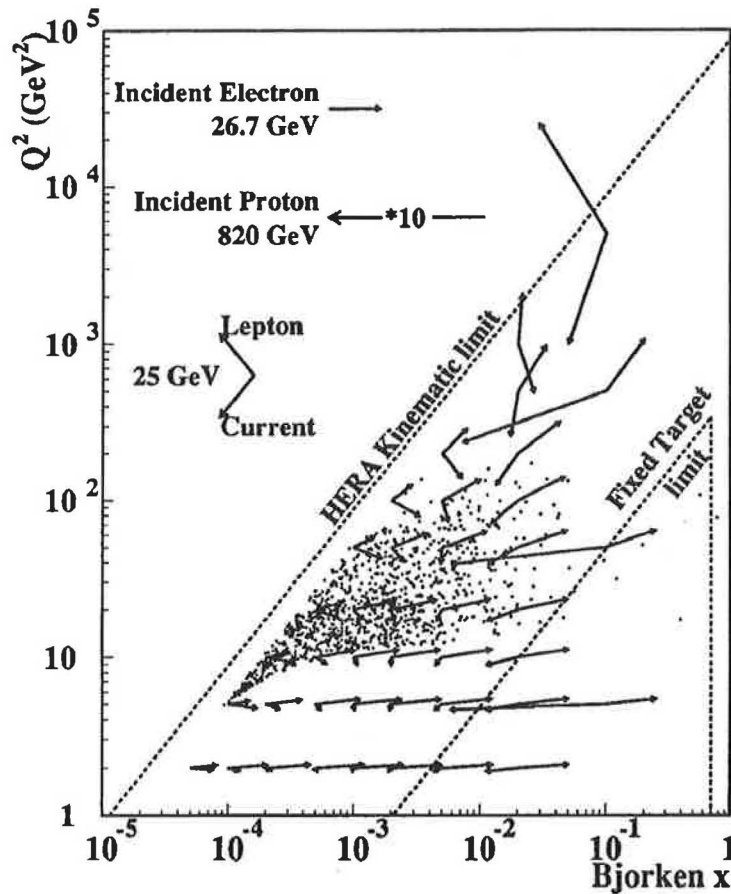


FIG 9: Lepton-current parton scattering kinematics in the $x_{Bj} - Q^2$ plane at HERA: note the different energy scales for the upper lepton and lower jet vectors; also superimposed is the 1992 H1 DIS event sample showing the first experimental sensitivity to lepton-nucleon DIS at very low x_{Bj} .

DIS in H1

The 1992 H1 DIS data sample is restricted to Q^2 measured in the BEMC because of limited statistics. This is clear in FIG. 9 which, as well as showing the coverage in Q^2 and x_{Bj} , also shows how the final state hadronic energy flow can swing about the whole acceptance of the H1 detector. The lower limit contour in Q^2 is essentially that of the beam pipe cut ($\theta < 172.5^\circ$) for the electron. The relationship between scattered electron energy $E_{e'}$ and Bjorken- x x_{Bj} (see equations (2) and (3) above) at fixed (backward) scattering angle θ gives rise to a Jacobian peak as $E_{e'} \rightarrow E_e$ (and $y \rightarrow 0$) in the distribution of $E_{e'}$ irrespective of anything but the most violent dependence of the DIS rate on x_{Bj} (or for that matter $\log_{10} x_{Bj}$). This is loosely referred to as the “kinematic

peak" at $E_e' = E_e$. It provides a useful self-calibrating cross check of the energy scale of the BEMC in the DIS sample.

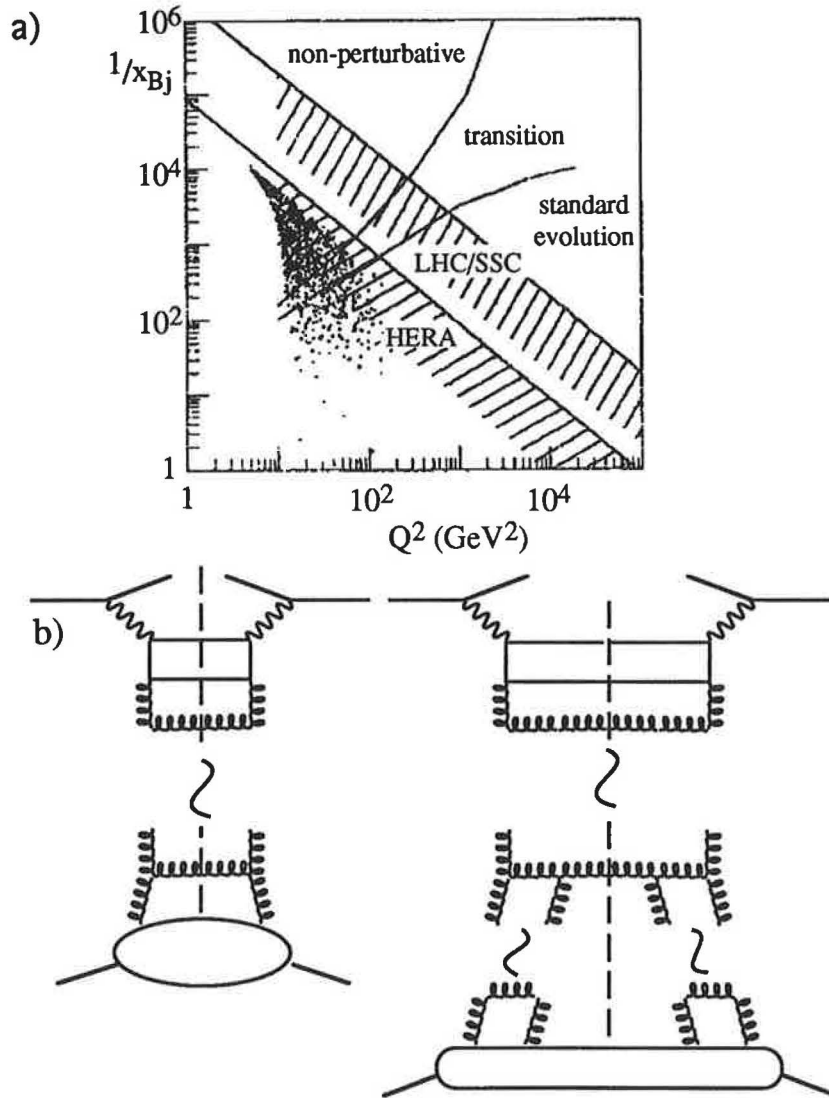


FIG 10: a) Theoretical prejudice concerning QCD, and the proton structure function F_2 in the $1/x_{Bj} - Q^2$ plane; "standard evolution" refers to perturbative DGLAP evolution, and "transition" and "non-perturbative" refer to new unmeasured domains where there is at least uncertainty about the viability of DGLAP evolution; the sensitivity of deep inelastic physics at HERA and at SSC/LHC in this plane are also marked, and the first DIS sample from H1 superimposed; b) gluon dominated QCD diagrams ("ladder" and "fan" diagrams) which are important contributions to F_2 and (when cut!) to DIS energy flow in the new low x_{Bj} region accessed for the first time by HERA data.

FIG. 11 summarises how the data collection and analysis proceeds by reference to the scattered electron energy spectrum. The measured trigger rate in the BEMC is reduced by a factor 100 using the tight ToF timing. Off-line electron identification and reconstruction results in the E_e' spectrum in which the "kinematic peak" is obvious. The spectrum consists of genuine DIS electrons contaminated increasingly as E_e' decreases by the "tail" of misidentified hadrons from photoproduction events in which the electron escapes down the beam pipe. How

one places a cut on $E_{e'}$ so as to reduce the photoproduction contamination to manageable levels without cutting too much into lower x_{Bj} measurements is a matter of trade-off between statistics and signal-to-background.

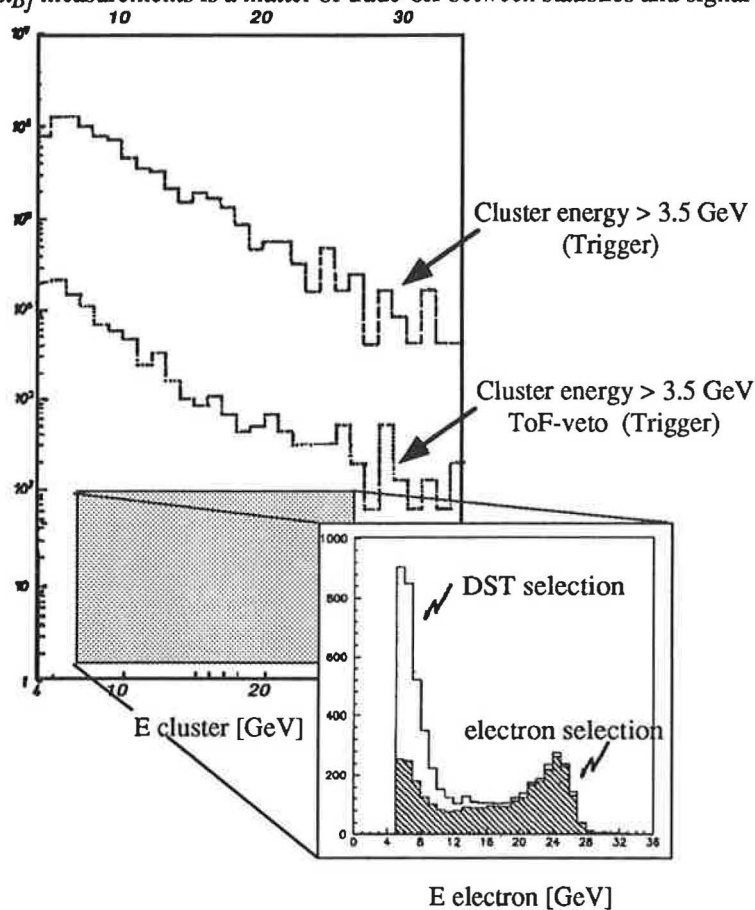


FIG 11: Outline of the extraction of a sample of DIS electrons in the BEMC Q^2 region: the cluster energy spectrum above 3.5 GeV is reduced to $\sim 1\%$ using the ToF cut against upstream out of time proton initiated background (log scale); on-line (L4) and off-line reconstruction cuts and checks to establish a DIS sample yield the candidate scattered electron energy spectrum (linear scale) which includes hadrons from remaining photoproduction background; the latter is then further reduced with cuts on shower shape, energy and position in the BEMC; the resulting electron energy spectrum shows a “kinematic peak” at approximately beam energy.

In contrast with fixed target DIS experiments, the reconstruction of the important kinematic variables Q^2 and x_{Bj} follows not only from the reconstruction of the scattered electron and equations (2), (3) and (4). The typical reconstruction errors mean that, both for very backward electrons at small scattering angles (near the beam pipe - $\pi - \theta$ small) and for electrons with scattered energy $E_{e'}$ close to initial energy E_e , i.e. close to the kinematic peak, y from equation (2) is very badly determined. One then also turns to the final state hadrons for which

$$y = (E_{had} - P_{zhad})/2E_e \quad (7)$$

is now a good measure of y , where E_{had} is the total hadronic energy and P_{zhad} is the total momentum component of the hadronic energy in the forward (proton) direction [23]. Determination of y using equations (2) and (7) nicely complement each other. Thus a large kinematic range in Q^2 and x_{Bj} is well measured with significant overlap between both determinations of y providing a check on systematic errors.

Measurement of the Low x_{Bj} Dependence of the Proton Structure Function F_2

The sample of DIS events has been used to extract the Q^2 and x_{Bj} dependences of the proton structure function F_2 . There are many technical details of the analysis which may be found in [24] including an exhaustive discussion of the systematic errors. Parallel analyses, one using only the scattered electron and the other using both the electron and the final state hadrons, yield consistent results where they overlap, despite the different sources of systematic error and the approaches to radiative corrections.

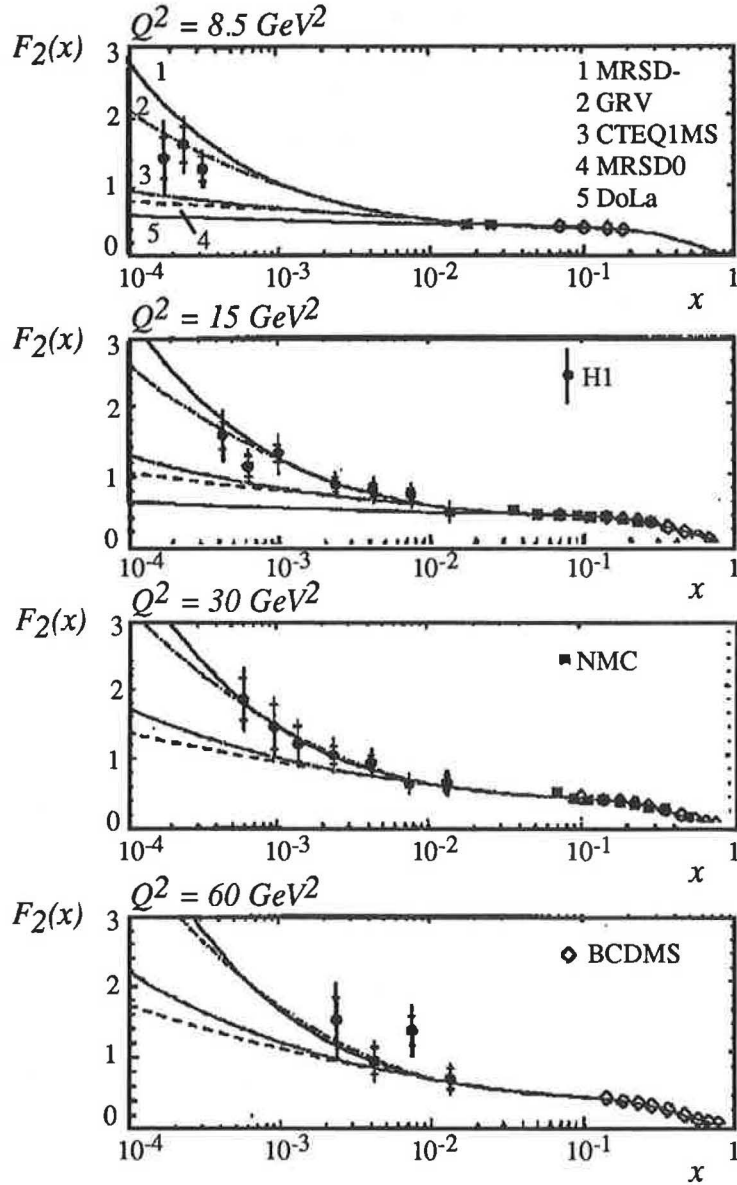


FIG. 12: The low x_{Bj} dependence of the proton structure function F_2 measured at four different Q^2 in the range 8.5 to 60 GeV^2 ; an overall systematic uncertainty in normalisation of 8% due to accuracy of luminosity measurement is not included; also shown are measurements from BCDMS [27] and NMC [28] at higher x_{Bj} and comparison with various theoretical expectation [25] based on extrapolation into the new low x_{Bj} region of fits to the BCDMS and NMC data.

The results are summarised in FIG. 12 [24]. A consistent and intriguing picture emerges from the x_{Bj} dependence measured at four different values of Q^2 in the range 8.5 to 60 GeV^2 , namely a large (\sim factor 2) increase of F_2 with decreasing x_{Bj} for $0.0001 < x_{Bj} < 0.012$. Also shown are previous measurements at larger x_{Bj} and a soupçon of theoretical expectation, most based largely on extrapolation of QCD analyses of substantial data at larger x_{Bj} but with some theoretical prejudice injected into the extrapolation [25]. Irrespective of the success or not of the latter, most of which anyway assume either DGLAP-like or Regge-like Q^2 and x_{Bj} dependences extrapolated into what may be a completely inappropriate kinematic region (FIG. 10), such a large increase (far from the only kinematic limit at $x_{Bj} = 1$) in the proton structure function F_2 is, at face value, a quite remarkable result with important and far-reaching implications for our understanding of hadron structure. This significant result has also been confirmed by the Zeus experiment [26].

The DIS Hadronic Final State

The DIS hadronic final state itself contains a wealth of information about proton sub-structure. The immense increase in ep collision energy at HERA, which is manifest in the increase of the phase space available

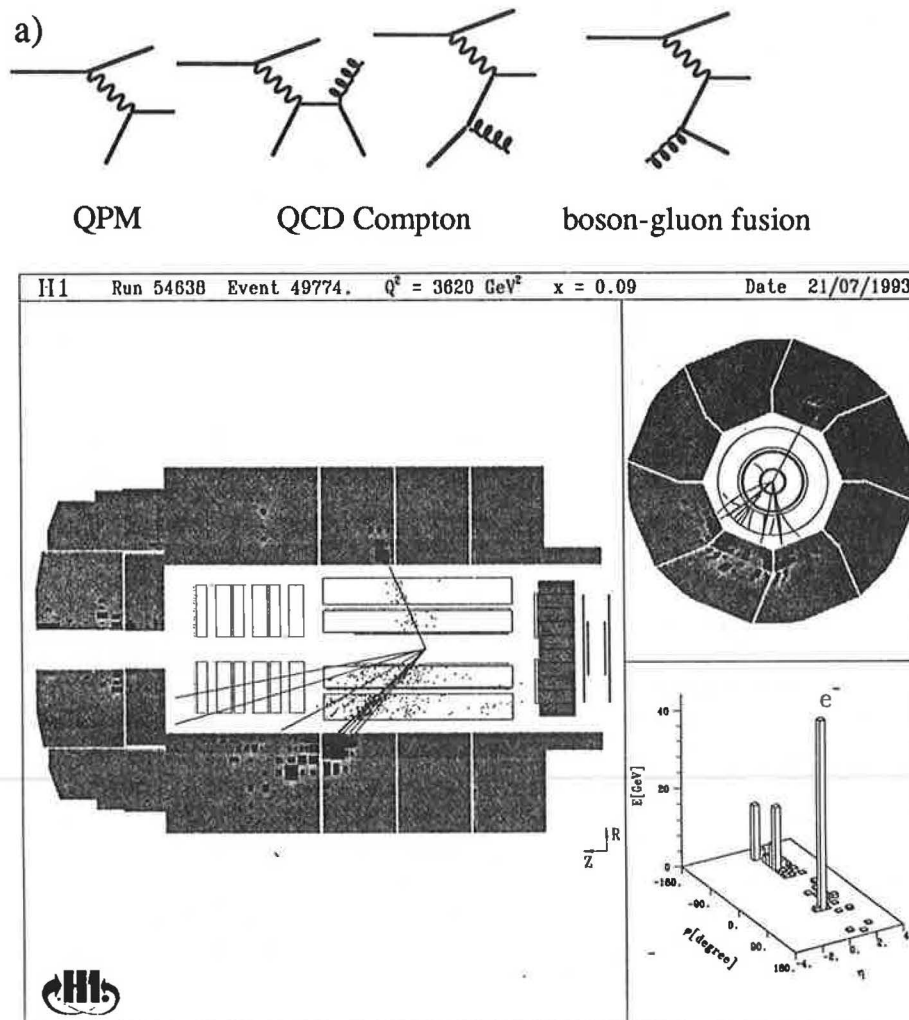


FIG. 13: a) QPM and QCD $O(\alpha_S)$ diagrams which give rise to jet production in DIS ep ; b) a (high Q^2) 2+1 jet candidate event in DIS in which some of the proton remnant jet is detected.

to the hadronic final state ($W \leq \sim 700 \text{ GeV}$ in present low x_{Bj} data), has meant that, for the first time in lepton nucleon DIS, jet production is now visually obvious. The leading topology for jet production at HERA (QPM in FIG. 13a) is of course 2-jet, 1 jet associated with the current quark and 1 associated with the proton remnant which is close to the beam pipe and at best is only partly detected - the 1+1 jet topology (FIG. 13b). Hard, high p_T , $O(\alpha_S)$ QCD corrections, namely QCD Compton and boson-gluon fusion (FIG. 13a), give rise to the 2+1 jet topology. FIG. 13b shows a 2+1 jet candidate event. Using the JADE jet algorithm [29] and the available QCD inspired Monte Carlo simulations of parton dynamics to correct for experimental bias [30], one can attempt to quantify the jet topology production rates R_{N+1} as fractions of the total sample. FIG. 14 summarises the result by showing R_{2+1} as a function of Q^2 and compared with expectation assuming α_S running (four flavour, $\Lambda=200 \text{ MeV}$) and α_S constant [31]. Note that a rising R_{2+1} is predicted despite the expectation of a running $\alpha_S(Q^2)$ because of the rapidly increasing phase space (increasing W) for the 2+1 jet fraction with increasing Q^2 at low x_{Bj} . Roughly speaking, 10 to 20% of events are of the 2+1 jet type, and one can anticipate that, with not much more data, it will be possible to demonstrate the Q^2 dependence of α_S in a single measurement.

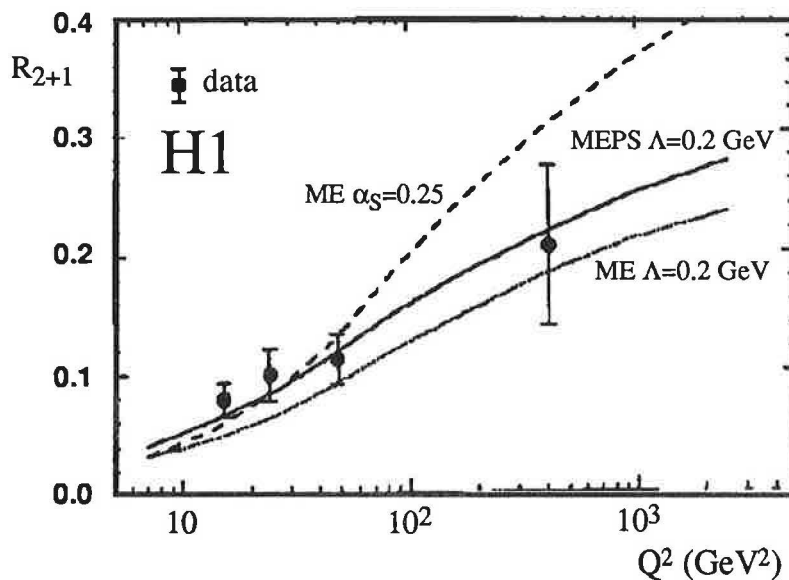


FIG.14: The fraction of 2+1 jet events R_{2+1} measured using the JADE algorithm as a function of Q^2 , together with the expectation of QCD based simulation [30] assuming a constant α_S and an asymptotically free α_S .

The QCD inspired simulations of parton induced hadronic final states, which have been well honed to all available low energy ep , e^+e^- and pp data, can also be compared directly with the DIS data [30]. The models take a variety of different approaches and inevitably include a number of different unknown or ill-defined parameters, some of which have been “tuned” on the available e^+e^- , pp and ep data, to control leading order QCD divergences and to specify color flow. It is thus interesting now to see how well, without any further honing, they reproduce the salient characteristics of the DIS final state in the new low x_{Bj} kinematic region of first HERA data.

In H1 all these models have been compared with DIS data without, wherever meaningfully possible, any significant adjustment of parameters. Of course the models are useless without the parton sub-structure in the proton, that is the QCD evolved F_2 , which is of course not yet well known in the new low x_{Bj} region of present data (see above), and for which therefore some assumption has to be made. With an estimate of systematic uncertainty of about 10% due to this caveat in mind, first comparisons with energy flow have already discriminated against certain theoretically motivated approaches to the choice of unknown parameters in the QCD based simulations [32].

An overall view of the present state of this considerable enterprise is in FIG. 15. The “sea gull” plot, in which charged track p_T with respect to the virtual photon-proton axis is studied as a function of Feynman x_F , is well known to be very sensitive to the details of parton hadronisation. The comparison with the models (including detector effects) is shown in FIG. 15a for positive x_F which focuses on hadronisation associated with

the current jet. There is some agreement, which is perhaps to be expected because the hadronisation of the time-like current quark in DIS is unlikely to differ from similar time-like quark hadronisation in e^+e^- interactions.

More interesting is to compare data and expectation in the phase space region between the struck quark (current) and the proton remnant where the hadronisation is due to color flow between the two, or equivalently is associated with initial state chromodynamic radiation (FIG. 10b). FIG. 15b shows the average weighted energy flow as a function of laboratory pseudorapidity η compared with some of the models. Discrepancies are now apparent in the forward (proton direction) hemisphere, which is not to say that the models should now be rejected - only that they have to be honed further to accommodate this completely new and fascinating domain of color flow and hadronisation.

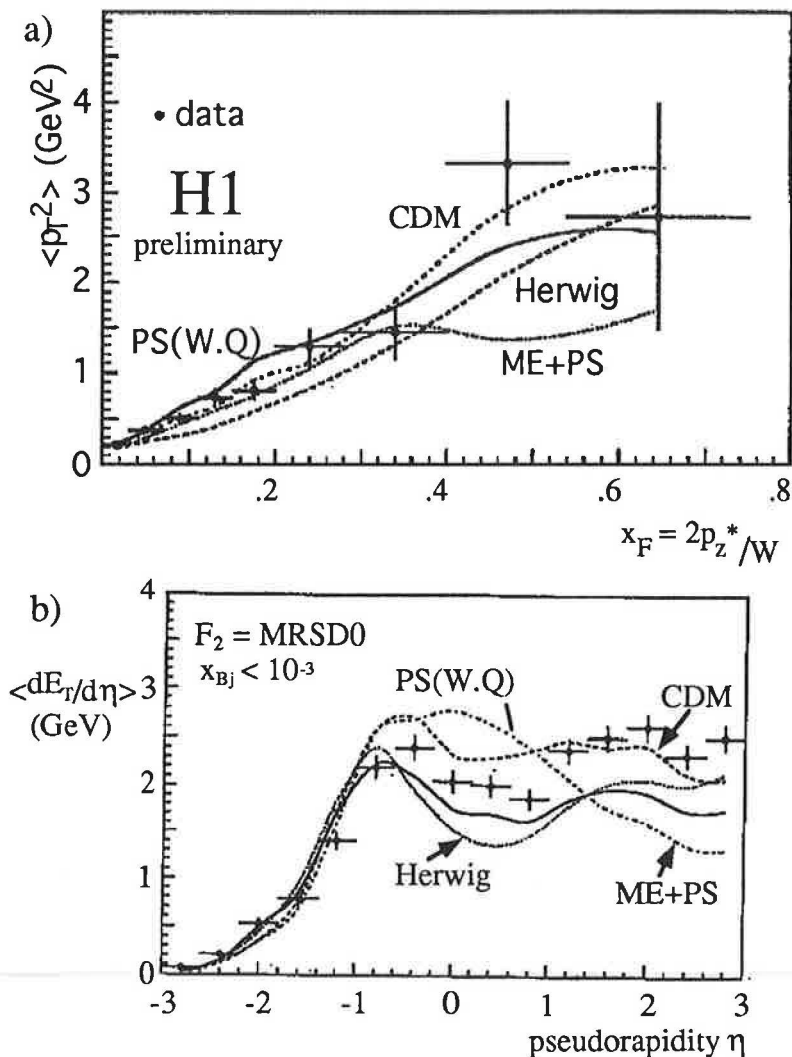


FIG. 15: a) "Sea gull" plot in which average charged track p_T with respect to the virtual photon-proton CMS axis is plotted as a function of Feynman x_F , together with the expectation of different QCD based models (uncorrected for experimental bias); b) average weighted energy flow $\langle dE_T/d\eta \rangle$ as a function of laboratory pseudorapidity η showing in the forward (proton direction - $\eta > 0$) hemisphere disagreement with these models.

Because of its richness and complexity, it is clear that we are a long way from a complete understanding of the DIS hadronic final state. However, despite this complexity, a significant feature of the DIS hadronic final state has emerged. In FIG. 16a is plotted the spectrum of rapidity intervals, measured with respect to the forward

edge of the LAr calorimeter, of the most forward energy cluster (energy > 400 MeV) in H1 DIS events. Comparison with any DIS simulation shows a clear excess of events with a rapidity gap larger than that expected in standard DIS simulation to date. Events with such a rapidity gap (with respect to the forward LAr limit) $\Delta\eta \geq 2$ amount to about 6% of all DIS, have a characteristically low measured hadronic mass M_X (FIG. 16b), and have Q^2 dependence consistent (to within large uncertainty due to limited statistics) with all DIS events shown when the ratio R of those with a rapidity gap to all is plotted as a function of Q^2 (to minimise effects due to experimental bias) (FIG. 16c). Similar results have been published by the Zeus experiment [33].

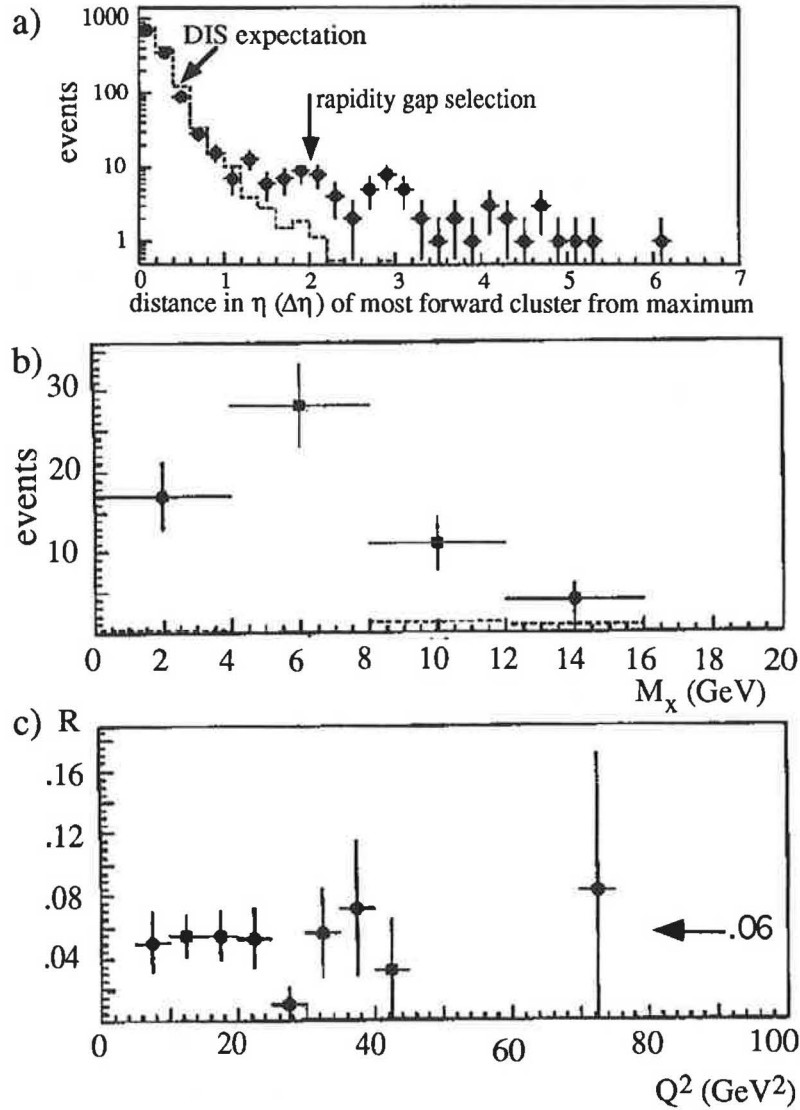


FIG. 16: a) Distribution of rapidity gap $\Delta\eta$ between the most forward (proton beam direction) final state hadronic cluster and the forward acceptance limit of the LAr calorimeter for all DIS events showing an excess over DIS expectation with $\Delta\eta$ greater than ~ 1.5 ; b) reconstructed hadronic mass M_X spectrum for all DIS events with a forward rapidity gap $\Delta\eta \geq 2$; c) fraction R of DIS $\Delta\eta \geq 2$ events in the total DIS sample as a function of Q^2 ; all spectra are uncorrected for experimental bias.

Any interpretation of events with a rapidity gap is built naturally on the break in the color flow between current quark and proton remnant which the gap demands (FIG. 10b). Given that the excess events observed have

rapidity gaps which extend to the most forward detectors, a natural temptation is to associate the sample with a color singlet proton remnant, such as a nucleon (p, n) or a low multiplicity (soft physics) jet of hadrons ($p\pi, n\pi, p\pi\pi, n\pi\pi, N^*, \Delta \dots$). This of course assumes no additional color flow in events in the rapidity regions between the operational forward detectors (down to $\eta \sim 3.5$) and the remnant in the beam pipe. In H1 there are a number of qualitative indications that this is likely to be the case. They include measurements with a partly instrumented plug calorimeter (down to $\eta \sim 5.5$, see FIG. 1), and the observation of a lower multiplicity of secondaries either in forward scintillators downstream of the experiment, or produced at collimators in the beam pipe by remnant particles which are then detected in the F μ detector (to $\eta \sim 6.6$, see FIG. 1).

Speculation as to an interpretation of such rapidity gap events serves to underline their significance in future developments of our understanding of DIS in terms of QCD. One could be tempted to the view that we are seeing DIS dynamics due to the color singlet "limbs" of the "fan diagram" of FIG. 10b. That such limbs have a theoretical interpretation associated with diffraction and the pomeron is well known [37]. A less pedagogical, but perhaps more exciting, way of saying this might be that the DIS probe is seeing color neutral sub-structure in the proton of size commensurate with its partonic spatial resolution - perhaps due to colorless clustering of the high density of gluons at low x_{Bj} ? An even less pedagogical view, which is born out by measurements at slightly lower Q^2 DIS in the form of elastic vector meson production [34], is that there is still to be found, even at these relatively high Q^2 , diffractive dissociation which is so important in hadronic physics. Until we have more data, it is too early to say more.

Search for Phenomena beyond the Standard Model and very high Q^2 DIS

The whole final state phase for DIS at HERA, when taken together with the expectation that Standard Model physics will occur with predictably low rate at high Q^2 , is wide open to the observation of new electron-quark dynamics. This translates into a unique sensitivity at HERA for new, exotic phenomena introduced in attempts to bring the quark and lepton sectors in the Standard Model together. In particular, any production of new states, such as leptoquarks, leptogluons, or excited leptons formed either by the fusion of electrons with partons or by the electroweak excitation of electrons scattering inelastically off partons, will produce an anomalous high Q^2 signal by virtue of their more isotropic decay angular distributions compared with Standard Model t channel exchange (FIG. 17). For a parton (or boson) from the proton with fractional momentum x of its parent, the mass of the new excited state m is given by

$$m^2 = xs \quad (9)$$

and if the subsequent decay is elastic $x = x_{Bj}$. Thus new physics corresponding to the production of one such state will appear as an enhancement over expectation at fixed x_{Bj} , with, because of equations (4) and (5), a Q^2 distribution which will follow its decay angular distribution in $\cos \theta^*$, and therefore will be much more uniform than the Standard Model ($1/y^2$) expectation.

Based on only 25 nb^{-1} of data, no anomalies have been seen and significant new lower limits can be assigned to the invariant masses of putative leptoquarks ($\leq \sim 190 \text{ GeV}$ for coupling $\lambda = 0.3$) leptogluons ($\leq \sim 200 \text{ GeV}$), and R-parity violating supersymmetric squarks ($\leq \sim 170 \text{ GeV}$ for coupling $\lambda = 0.3$). For the production of excited electrons and neutrinos, upper limits on the production cross sections are quoted ($\leq 160 \text{ pb}$) [35].

Of course of more conventional interest is the achievement of a well understood Q^2 - x_{Bj} plane in terms of the Standard Model yield of DIS NC and CC physics. Data taking in 1993 has already provided integrated luminosity for which handfuls of CC events are expected. FIG. 18 shows one such event, characterised by its substantial p_T imbalance. It will soon be possible to make the first checks of Standard Model expectation not only in terms of CC rate but also in terms of CC event topology involving associated jet and charged lepton production. Equally spectacular, and just as significant, handfuls of NC events at these large and unprecedented Q^2 will also be available making possible the measurements of space-like γ - Z^0 interference.

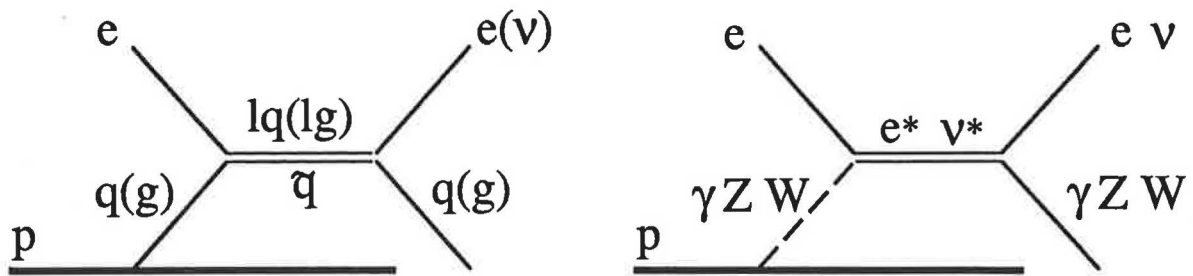


FIG. 17: Diagrams describing the formation of new electron-parton (leptoquark, leptogluon, R-parity violating squark) and electron-gauge boson (e^*) excited states which appear as anomalous rate in the Q^2 - x_{Bj} plane.

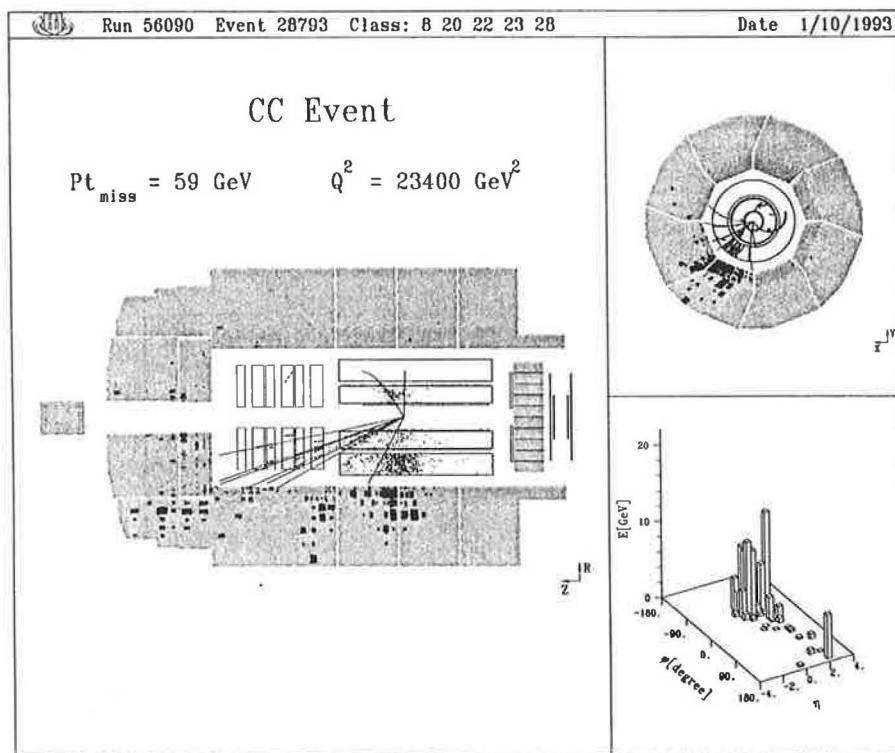


FIG. 18: DIS CC candidate event identified by substantial p_T imbalance visible in the r - ϕ projection; kinematic variables are $Q^2 = 23000 \text{ GeV}^2$ $x_{Bj} = 0.34$.

CONCLUSION

After the first 6 months of HERA operation for physics data taking at CM energy 296 GeV , H1 has analysed about 25 nb^{-1} of integrated luminosity. New results concerned both with photon and proton sub-structure and with new exotic sub-structure outside the Standard Model have been presented:

Photoproduction Physics at a new energy scale of $\langle W_{\gamma p} \rangle = 197 \text{ GeV}$:

- the total cross section is presently measured to be $156 \pm 2 \pm 18 \text{ (sys)} \mu\text{b}$

- for the first time high p_T jet production is unambiguously observed and the inclusive jet production cross section has been measured
- first evidence is presented for sensitivity of resolved photon processes both to photon structure and to gluon content in that structure.

Deep Inelastic ep Physics in a new kinematic region $0.0001 < x_{Bj} < 0.012$

- first measurement of the proton structure function F_2 has been made revealing a substantial increase with decreasing x_{Bj}
- first comparisons have been made of the hadronic final state with QCD expectations based on established parton simulations, and interesting discrepancies have already emerged
- a class of events, whose interpretation remains unclear, with a large rapidity interval which is devoid of any hadronic energy flow around the downstream proton beam direction and which could extend down to the proton remnant, has been observed.

Deep Inelastic ep Physics in the new high Q^2 kinematic region at HERA

- first observations in this new domain of deep inelastic neutral and charged current events have been made
- significant new upper limits on production of leptoquarks, leptogluons (masses $< \sim 190 \text{ GeV}$) and excited electrons and neutrinos outside the framework of the Standard Model have been established.

ACKNOWLEDGEMENTS

None of the physics which I have presented here would have been possible without the immense efforts of very many people. The initial operation of the unique collider facility HERA and its extremely quick commissioning for luminosity running are due to the dedication and skill of the few who constitute the machine group at DESY. The construction and commissioning of H1 is in large part due to similar dedication, skill and determination by engineers and technicians in all the H1 collaborating institutes since 1986. The on-going operation, data taking, and data analysis work is in the expert hands of all my colleagues in H1, with whom it is always a pleasure to work.

REFERENCES

1. H1 Collaboration, Letter of Intent, DESY 1985.
2. H1 Collaboration, Technical Proposal, DESY 1986.
3. H1 Collaboration, "The H1 Detector at HERA", DESY 93-103 (1993)
4. B. Andrieu et al (The H1 Calorimeter Group), "The H1 Liquid Argon Calorimeter System", accepted for publication in Nucl. Inst. Meth., DESY 93-078 (1993)
5. R. J. Apsimon et al (WA69 Collaboration), Z. Phys. C 43, 63 (1989)
6. Early theoretical work on the hadronic photon structure function F_2 :
T. F. Walsh, P M Zerwas, Nucl. Phys. B 41, 551 (1972)
R. L. Kingsley, Nucl. Phys. B 60, 45 (1973)
E. Witten, Nucl. Phys. B 120, 189 (1977)
Ch. Llewellyn Smith, Phys. Lett. 79 B, 83 (1978)
R. J. DeWitt, L. M. Jones, J. D. Sullivan, D. E. Willen, H W Wyld Jr, Phys. Rev. D 19, 2046 (1979)
W. R. Frazer, J. F. Gunion, Phys. Rev. D 20, 147 (1979)
C. T. Hill, G. G. Ross, Nucl. Phys. B 148, 373 (1979)
C. Petersen, T. Walsh, P. M. Zerwas, Nucl. Phys. B 174, 424 (1980)
7. D. Miller, "Low Energy QCD Studies", talk in these proceedings, and references therein
First precision measurement of the hadronic photon structure function F_2 :
Ch. Berger et al, Phys. Lett. 142 B, 111 (1984) 111
8. F. Eisele, "First Results from H1", in Proceedings of the 26th International Conference on High Energy Physics, Dallas, August 1992, p 2048, ed. J. R. Sanford (1992), DESY 92-140 (1992)
T. Ahmed et al. (H1 Collaboration), Phys. Lett. B 297, 205 (1992)

9. T. Ahmed et al. (H1 Collaboration), Phys. Lett. B 299, 374 (1993)
10. M. Derrick et al (Zeus Collaboration), Phys. Lett. B 293, 465 (1991)
11. A. Donnachie, P. V. Landshoff, CERN-TH 6635/92 (1992)
12. H. Abramowicz et al, Phys. Lett. B 269, 465 (1991)
13. I. Abt et al. (H1 Collaboration), Phys. Lett. B 314, 436 (1993)
14. F. M. Borzumati, B. A. Kniehl, G. Kramer, "Inclusive Particle Production at HERA: Higher Order QCD Corrections to the resolved quasi-real photon contribution", DESY 93-034 (1993)
15. C. Albajar et al. (UA1 collaboration), Nucl. Phys. B 335, 261 (1990)
16. J. E. Huth et al, "Towards a Standardisation of Jet Definitions", Fermilab-conf-90/249-E (1990)
17. M. Glück, E. Reya, A. Vogt (GRV), Phys. Rev. D 46, 1973 (1992)
H. Abramowicz, K. Charchula, A. Levy (LAC2, LAC3), Phys. Lett. B 269, 458 (1991)
L. E. Gordon, J. K. Storrow, Phys. Lett. B 291, 320 (1992)
18. S. Bethke, "Tests of QCD" in Proceedings of the 26th International Conference on High Energy Physics, Dallas, August 1992, p 81, ed. J. R. Sanford (1992), and J Bartels, DESY 92-114
19. Yu. L. Dokshitzer, JETP 46, 641 (1977)
V. N. Gribov and L. N. Lipatov, Sov. Journ. Nucl. Phys. 15, 78 (1972)
G. Altarelli and G. Parisi, Nucl. Phys. B 126, 298 (1977)20.
20. A. Mueller, Nucl. Phys. B (Proc.Suppl.) 18C, 125 (1990)
A. Mueller, Nucl. Phys. B (Proc.Suppl.) 29A, 275 (1992)
21. E. A. Kuraev, L. N. Lipatov and V. S. Fadin, Sov. Phys. JETP 45, 199 (1977)
Ya. Balitsky and L. N. Lipatov, Sov. J. Nucl. Phys. 28, 822 (1978)
22. Proceedings of the Phenomenology Workshop "HERA - the new frontier for QCD", ed. J. B. Dainton, R. Devenish, R. G. Roberts, to be published in J. Phys. G.
23. A. Blondel and F Jacquet, Proceedings of a Study of an ep facility for Europe, ed. U. Amaldi, DESY 79-48, 391 (1979)
24. I. Abt et al. (H1 Collaboration), Nucl. Phys. B407 (1993) 515-535
25. A. D. Martin, W. J. Stirling, R. G. Roberts (MRSD0, MRSD-), Phys. Lett. B 306, 145 (1993), *ibid* B 309, 492 (1993)
J. Botts et al (CTEQ1MS), Phys. Lett. B 304, 159 (1993)
M. Glück, E. Reya, A. Vogt (GRV), Z. Phys. C 53, 127 (1992)
M. Glück, E. Reya, A. Vogt (GRV), Phys. Lett. B 306, 391 (1993)
A. Donnachie, P. V. Landshoff (DoLa), M/c-th 93/11, DAMTP 93-23 (1993)
26. M. Derrick et al (Zeus Collaboration), "Measurement of the Proton Structure Function F_2 in ep scattering at HERA", accepted for publication in Phys. Lett., DESY 93-110 (1993)
J. F. Martin, "Results from the Zeus Collaboration", talk in these proceedings
27. A. C. Benvenuti et al (BCDMS Collaboration), Phys. Lett. B 223, 485 (1989)
28. P. Amaudruz et al (NMC Collaboration), Phys. Lett. B 295, 159 (1992), and erratum to CERN-PPE/92-124 CERN (1993)
29. W. Bartel et al (JADE Collaboration), Z. Phys. C 33, 23 (1986)
30. G. Ingelman, "LEPTO 6.1", in Proc. of Workshop "Physics at HERA", ed. W. Buchmüller and G. Ingelman, Hamburg (1991), p 1366, Vol. 3
T. Sjöstrand, Comp. Phys. Comm. 39, 347 (1986)
T. Sjöstrand and M. Bengtsson, Comp. Phys. Comm. 43, 367 (1987)
T. Sjöstrand, "JETSET 7.3", CERN-TH-6488-92 (1992)
L. Lönnblad, Comp. Phys. Comm. 71, 15 (1992)
G. Marchiesini et al, Comp. Phys. Comm. 67, 465 (1992) and references therein
31. I. Abt et al. (H1 Collaboration), "A measurement of multi-jet rates in DIS at HERA", DESY 93-137, October 1993, accepted for publication in Z. Phys. B
32. T. Ahmed et al (H1 Collaboration), Phys. Lett. B 298, 469 (1993)
33. M. Derrick et al (Zeus Collaboration), Phys. Lett. B 315, 481 (1993)
34. J. Ashman et al (EMC Collaboration), Z. Phys. C 39, 169 (1988)
P. Amaudruz et al (NMC Collaboration), Z. Phys. C 54, 239 (1992)

